Supplementary material

Development of an image Mean Square Displacement (iMSD)-based method as a novel approach to study the intracellular trafficking of nanoparticles

Luca Digiacomo[a,b], Michelle A. Digman[c], Enrico Gratton[c], Giulio Caracciolo[a,*]

[a] *Department of Molecular Medicine, Sapienza University of Rome, Viale Regina Elena 291, 00161 Rome, Italy*
[b] *Department of Bioscience and Biotechnology, University of Camerino, Via Gentile III da Varano, 62032 Camerino, (MC), Italy*
[c] *Laboratory for Fluorescence Dynamics, Biomedical Engineering Department, University of California at Irvine, Irvine, CA 92697, USA*

Contents

S.1. Decoupling of flow terms

The dynamics of many particles undergoing Brownian diffusion + flow motion in a two-dimensional space is described by a diffusion coefficient D and a driving speed $\vec{v}$. In general, the particles move along different directions, since the flow speed can be distributed over a plane. This leads to an angular spread of particle displacements from their starting positions (Fig. S.1). If the speed strength $v = |\vec{v}|$ is supposed to be the same for each particle, then the flow motion can be described in terms of the following statistical moments:

$$\vec{v}_\phi = \langle \vec{v} \rangle \tag{S.1}$$

$$v_\sigma^2 = \langle (\vec{v} - \langle \vec{v} \rangle)^2 \rangle \tag{S.2}$$

where the former is a vectorial average over the ensemble and the latter represents the corresponding mean square displacement. Furthermore, v_σ^2 can be expressed as

$$v_\sigma^2 = \langle (\vec{v} - \langle \vec{v} \rangle)^2 \rangle = \langle \vec{v}^2 - 2\vec{v}\langle \vec{v} \rangle + \langle v \rangle^2 \rangle = \langle \vec{v}^2 \rangle - 2\langle \vec{v} \rangle^2 + \langle \vec{v} \rangle^2 = \langle \vec{v}^2 \rangle - \langle \vec{v} \rangle^2 \tag{S.3}$$

Finally, under the assumption of constant speed's modulus, $\langle \vec{v}^2 \rangle = \langle v^2 \rangle = v^2$ and the following relationship is obtained:

$$v^2 = v_\phi^2 + v_\sigma^2 \tag{S.4}$$

*Corresponding author
Email address: giulio.caracciolo@uniroma1.it (Giulio Caracciolo)

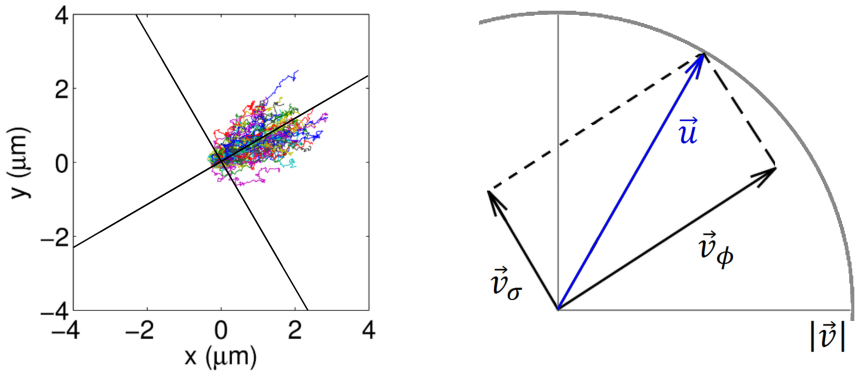

Figure S.1: Particle displacements from starting positions for dynamics driven by Brownian diffusion + uniformly distributed flow motion and scheme of the adopted speed's decomposition.

In other words, $\vec{v}_\phi$ defines the resulting average speed of the ensemble and v_σ^2 quantifies a spread along the orthogonal direction with respect to the particle flow. This decomposition is useful to study the effect of the angular distribution of the velocities on the spatiotemporal correlation function. Indeed, fluorescence correlation analysis should take into account the overall behaviour arising from single-particle dynamics.

According to the iMSD theory the spatiotemporal correlation function can be written as (Di Rienzo et al. Nature Communications 5, 2014)

$$g(\xi,\eta,\tau) = g_0\, p(\xi,\eta,\tau) \otimes W(\xi,\eta) \tag{S.5}$$

where g_0 defines the contrast of fluctuation and is related to the average number of particles in the observation volume, $W(\xi,\eta)$ represents the instrument Point Spread Function (PSF) and $p(\xi,\eta,\tau)$ is the probability function describing the dispersive dynamics. p is related to the single particle transition probability, i.e. probability that a single particle originally at $\vec{r}$, will be at $\vec{r}\,'$ after a time period $\tau = t' - t$. For Brownian diffusion + directed motion, it can be expressed by the following equation:

$$P(\vec{r}\,'|\vec{r},\tau) = \frac{1}{4\pi D\tau} \exp\left\{-\frac{|\vec{r}\,' - \vec{r} - \vec{v}\tau|^2}{4D\tau}\right\} \tag{S.6}$$

where D is the diffusion coefficient and $\vec{v}$ uniquely defines direction and strength of the directed motion of that particle. As a consequence, when particles are driven along the same direction, the spatiotemporal correlation function can be written as

$$g(\vec{\rho},\tau)\Big|_{\psi=0} = G_\infty + G_1(\tau)\exp\left\{-\frac{(\vec{\rho} - \vec{v}\tau)^2}{\omega^2 + 4D\tau}\right\} \tag{S.7}$$

where $\vec{v} = \langle\vec{v}\rangle = \vec{v}_\phi$ and $\langle(\vec{v} - \langle\vec{v}\rangle)^2\rangle = 0$. Under this assumption, $g(\vec{\rho},\tau)$ can be fitted by a Gaussian function, whose peak uniformly drifts and variance linearly increases with time. However, when the

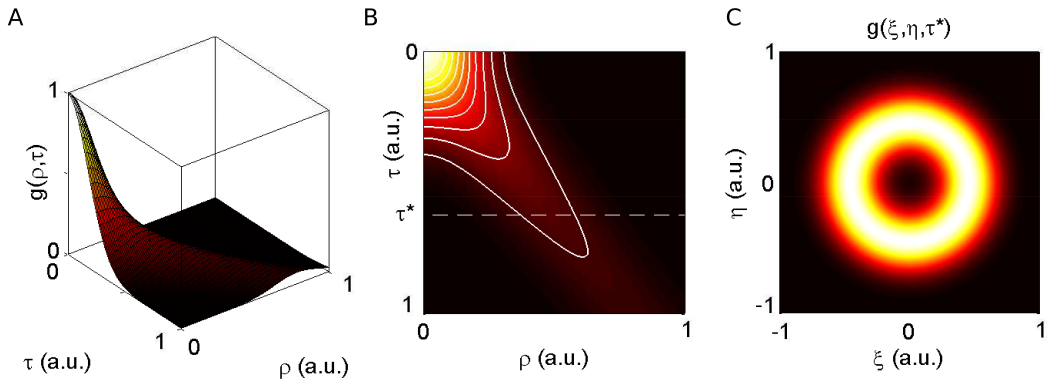

Figure S.2: (A) 3D view, (B) top view and contour plot of the analytic relationship S.11, as function of ρ and τ. (C) Corresponding representation over the spatial lag domain at high time lag (rescaled color units).

particle speed is distributed over an angular range ψ, the resulting correlation function is obtained by averaging Eq. S.7 over the ensemble, i.e.

$$g(\vec{\rho},\tau)\Big|_{\psi} = G_\infty + G_1(\tau)\left\langle \exp\left\{-\frac{(\vec{\rho}-\vec{v}\tau)^2}{\omega^2+4D\tau}\right\}\right\rangle \tag{S.8}$$

Furthermore, since in polar coordinates $\vec{\rho}=(\rho\cos\theta;\rho\sin\theta)$ and $\vec{v}$ can be expressed as

$$\vec{v} = \begin{cases} \begin{pmatrix} v\cos\theta' \\ v\sin\theta' \end{pmatrix} & -\frac{\psi}{2} < \theta' < \frac{\psi}{2} \\ 0 & \text{otherwise} \end{cases} \tag{S.9}$$

the ensemble average in Eq. S.8 can be carried out as angular average, as follows

$$\begin{aligned} g(\rho,\theta,\tau,\psi) = G_\infty + \frac{G_1(\tau)}{\psi}\exp\left\{-\frac{\rho^2+v^2\tau^2}{\omega^2+4D\tau}\right\}\times \\ \times\int_{-\psi/2}^{\psi/2}\exp\left\{\frac{2\rho v\tau}{\omega^2+4D\tau}\cos(\theta'-\theta)\right\}\mathrm{d}\theta' \end{aligned} \tag{S.10}$$

Where θ and θ' are counted from the mean direction of the flow. When particle speed is symmetrically distributed, i.e. for $\psi=2\pi$, Eq. S.10 admits the following analytic solution:

$$g(\rho,\tau)\Big|_{\psi=2\pi} = G_\infty + G_1(\tau)\exp\left\{-\frac{\rho^2+v^2\tau^2}{\omega^2+4D\tau}\right\} I_0\left(\frac{2\rho v\tau}{\omega^2+4D\tau}\right) \tag{S.11}$$

where I_0 is the zero order modified Bessel function of the first kind, whose expression can be written as (Abramowitz and Stegun 1972, p. 376):

$$I_0(z) = \frac{1}{\pi}\int_0^\pi e^{z\cos(\alpha)}\mathrm{d}\alpha \tag{S.12}$$

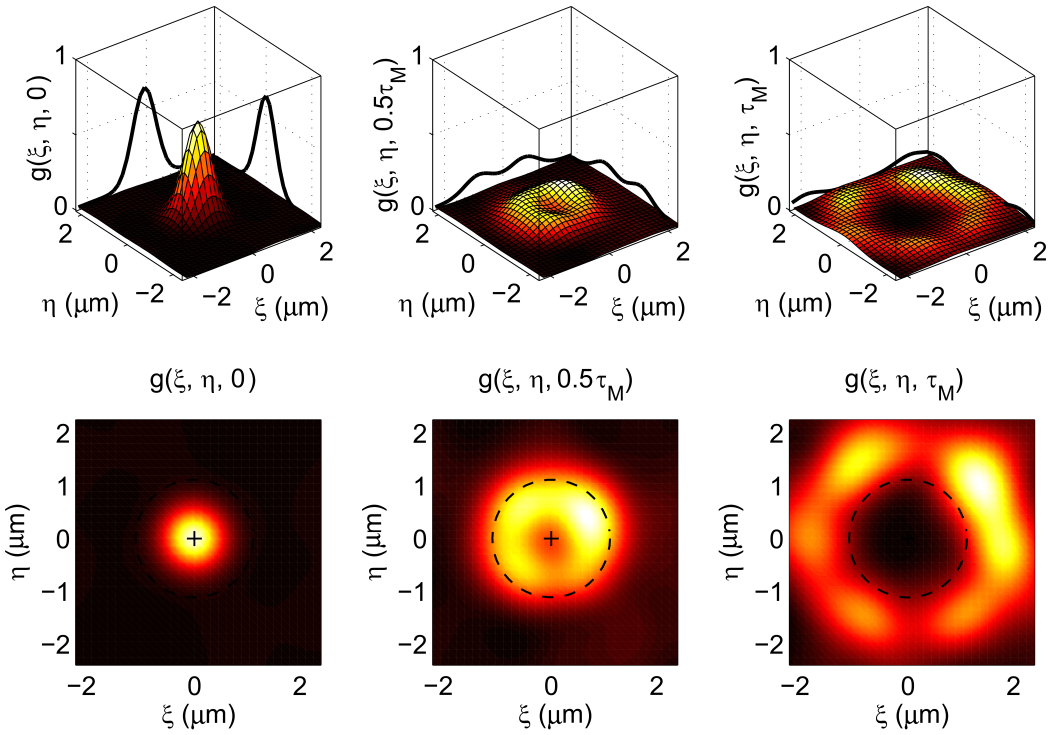

Figure S.3: Time evolution of the spatiotemporal correlation function describing isotropically distributed flow motion. The computation from numeric simulation has been carried out from $\tau = 0$ to a maximum time lag τ_M. Black solid lines represent the sections of the fitting function S.11 with the planes $\xi = 0$ and $\eta = 0$.

As expected, for $\psi = 2\pi$ the system is isotropic and the correlation function does not depend on θ. A graphic representation of Eq. S.11 is given in Fig. S.2 (panels A and B), for fixed values of ω, D and v. Of note, for $\tau = 0$, $g(\rho, 0)$ monotonically decreases, however there exist infinitely τ^* values such that $g(\rho, \tau^*)$ increases with ρ until a maximum is reached and then asymptotically decreases toward G_∞. This trend is depicted in Fig. S.2C, in cartesian coordinates: for $\psi = 2\pi$ the correlation function is symmetric with respect to the origin, from which radial Gaussian profiles move away, thus leading to a circular depression.

The aforementioned model has been validated by numeric simulations. Fig S.3 shows a representative example. The time evolution of the computed correlation function agrees with the expected theoretical trend, subsequently D, v and ω can be obtained as fitting parameters from Eq. S.11. In detail, at short timescale Eq. S.11 is not distinguishable from a Gaussian function. As an instance, at zero time lag, $I_0(0) = 1$ and $g(\rho, 0) = G_\infty + G_1 \exp(-\rho^2/\omega^2)$. At longer timescale, a circular depression is formed at the origin and maxima of g are distributed along a circumference of radius $v\tau$. The maximum time lag, for which a Gaussian approximation is valid can be quantified as follows. Any section of g on a plane orthogonal to (ξ, η) containing the origin can be viewed as a linear combination of two Gaussian curves drifting toward opposite directions and linearly spreading with τ (Fig. S.4). Indeed, each curve represents a single particle contribution, whose dynamic is driven

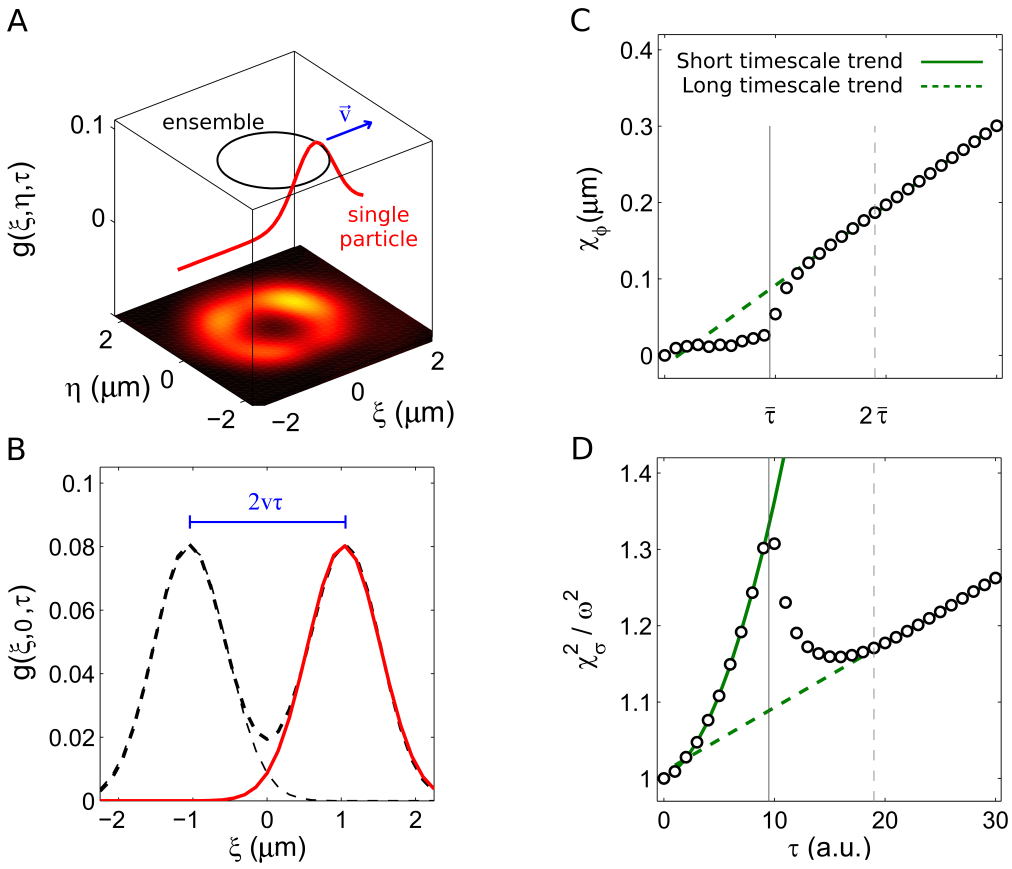

Figure S.4: (A) Schematic representation of the correlation function arising from single particle contributions and projection on the plane $\eta = 0$. (B) Fitting parameters as functions of τ and corresponding trends at short and long timescale.

by the transition probability given in Eq. S.6. The largest time $\bar{\tau}$, for which the spatial distance between the two peaks is smaller than the spread at that time lag, defines the upper limit of the short timescale, i.e.

$$2v\bar{\tau} = \sqrt{\omega^2 + 4D\bar{\tau}} \tag{S.13}$$

By adopting the usual definitions of the characteristic diffusion decay time and flow time ($\tau_d = \omega^2/(4D)$ and $\tau_f = \omega/v$, respectively), the curves are not distinguishable when

$$\tau < \bar{\tau} = \frac{\tau_f^2}{8\tau_d}\left(1 + \sqrt{1 + \frac{4\tau_f^2}{\tau_d^2}}\right) \tag{S.14}$$

Incidentally, when the diffusion is negligible with respect to the flow, i.e. for $\tau_f/\tau_d \ll 1$, the

Gaussian approximation is valid for

$$\tau < \frac{1}{2}\tau_f = \lim_{\tau_f/\tau_d \to 0} \bar{\tau} \tag{S.15}$$

On the other end, with similar arguments we can infer that particles contributions are fully distinguished for $\tau > \bar{\tau}$.

Fig S.4B shows the main outcomes of the above discussion. As prescripted by Eq. S.11, the spatiotemporal correlation function has been fitted by the following function:

$$g(\rho,\tau)\Big|_{\psi=2\pi} = \chi_\infty + \chi_1 \exp\left\{-\frac{\rho^2+\chi_\phi^2}{\chi_\sigma^2}\right\} I_0\left(\frac{2\rho\chi_\phi}{\chi_\sigma^2}\right) \tag{S.16}$$

where χ_∞, χ_1, χ_ϕ and χ_σ^2 represent the fitting parameters. As expected, at long timescale linear trends of χ_ϕ and χ_σ^2 have been found, with

$$\begin{cases} \chi_\phi = v\tau \\ \chi_\sigma^2 = \omega^2 + 4D\tau \end{cases} \quad \tau > 2\bar{\tau} \tag{S.17}$$

Therefore, in this regime Eq. S.21 is equal to the general form given in Eq. S.11. On the other side, at short timescale, the fitting procedure returns negligible values of χ_ϕ and a parabolic trend of χ_σ^2. Specifically, it has been found that

$$\begin{cases} \chi_\phi \simeq 0 \\ \chi_\sigma^2 = \omega^2 + 4D\tau + v^2\tau^2 \end{cases} \quad \tau < \bar{\tau} \tag{S.18}$$

Thus, in this regime the correlation function can be viewed as a Gaussian function of variance

$$\sigma^2(\tau) = \omega^2 + 4D\tau + v^2\tau^2 \tag{S.19}$$

This trend can be predicted by a Taylor expansion of the general theoretical relationship S.11 at $(0,0)$. Indeed, by imposing

$$G_2(\tau) = G_1(\tau) \exp\left\{-\frac{v^2\tau^2}{\omega^2+4D\tau}\right\} \tag{S.20}$$

Eq. S.11 reads

$$g(\rho,\tau)\Big|_{\psi=2\pi} = G_\infty + G_2 \exp\left\{-\frac{\rho^2}{\omega^2+4D\tau}\right\} I_0\left(\frac{2\rho v\tau}{\omega^2+4D\tau}\right) \tag{S.21}$$

Thus, the exponential term in Eq. S.21 can be approximated as follows:

$$\exp\left\{-\frac{\rho^2}{\omega^2+4D\tau}\right\} = 1 - \frac{\rho^2}{\omega^2+4D\tau} + \frac{\rho^4}{2(\omega^2+4D\tau)^2} + o(\rho^6+\tau^6) \tag{S.22}$$

and the series expansion of the Bessel function reads

$$I_0\left(\frac{2\rho v\tau}{\omega^2+4D\tau}\right) = 1 + \frac{v^2\tau^2\rho^2}{(\omega^2+4D\tau)^2} + \frac{v^4\tau^4\rho^4}{4(\omega^2+4D\tau)^4} + o(\rho^6+\tau^6) \tag{S.23}$$

Hence, by inserting Eq. S.22, S.23 in Eq. S.21,

$$g(\rho,\tau)\Big|_{\psi=2\pi} = G_\infty + G_2\left[1 - \frac{\rho^2}{q_1(\tau)} + \frac{\rho^4}{2q_2^2(\tau)} + o(\rho^6+\tau^6)\right] \tag{S.24}$$

where

$$\begin{cases} q_1(\tau) = \dfrac{(\omega^2+4D\tau)^2}{\omega^2+4D\tau-v^2\tau^2} \\ q_2(\tau) = \dfrac{\sqrt{2}(\omega^2+4D\tau)^2}{\sqrt{v^4\tau^4-4v^2\tau^2(\omega^2+4D\tau)+2(\omega^2+4D\tau)^2}} \end{cases} \tag{S.25}$$

Finally, the MacLaurin expansions of q_1 and q_2 lead to the following identities:

$$q_1(\tau) = \omega^2 + 4D\tau + v^2\tau^2 + o(\tau^4) = q_2(\tau) \tag{S.26}$$

Thus, $q_1 \simeq q_2 \simeq \sigma^2$ and Eq. S.24 can be viewed as the series expansion of a Gaussian function of variance $\sigma^2 = \omega^2+4D\tau+v^2\tau^2$. In conclusion, the spatial mean square displacement $\langle(\vec{v}-\langle\vec{v}\rangle)^2\rangle\tau^2 = v^2\tau^2$ contributes to the Gaussian variance with an additive term, which take into account that single particles isotropically move from their starting positions. Furthermore, at short timescale no peak's shift is revealed, since each single particle's drift along a direction is balanced by the opposite one: for $\psi = 2\pi$, $\langle\vec{v}\rangle = 0$.

Finally, when the particle speed is distributed within an angular range $\psi < 2\pi$, a peak's shift is revealed at short timescale, corresponding to the net resulting motion along the flow's direction. In turn, the mean square displacement decreases dependently on ψ (Eq. S.1, S.2, S.4). Thus, we can infer that under the Gaussian approximation, flow motion is responsible both for a drift term $\vec{v}_\phi\tau$ and a complementary spread contribution $v_\sigma^2\tau^2$, such that $g(\vec{\rho},\tau)$ can be approximated as

$$g(\vec{\rho},\tau) = G_\infty + G_1(\tau)\exp\left\{-\frac{(\vec{\rho}-\vec{v}_\phi\tau)^2}{\omega^2+4D\tau+v_\sigma^2\tau^2}\right\} \tag{S.27}$$

At longer timescale an angular spread become manifest. However, under the usual experimental conditions, the features of the investigated dynamics (i.e. the values of τ_d and τ_f) allow us to work within the Gaussian approximation's range and fully evaluate the flow terms in this regime.

S.2. Characterization of low-speed flow motion

The proposed approach aims to characterize Brownian diffusion + flow motion, by decoupling the speed contributions and by measuring diffusion coefficient and velocity. Although the drift contribution $\vec{v}_\phi$ is easily detected from the Gaussian peak's shift, measurements of v_σ can be tricky when the speed is low if compared with the diffusive term: i.e. when $\tau_f \gg \tau_d$. Under this condition, it may not be easy to recognize the parabolic term of the Gaussian's variance $\sigma^2(\tau)$. However it has been found that the iMSD procedure is in general more effective than the STICS one, which instead is focused on the trend of $g(0,0,\tau)$. Here we present two examples of fitting profiles, evaluated on numeric simulations mimicking the conditions $\tau_d/\tau_f = 0.12$ and $\tau_d/\tau_f = 0.06$. In the former situation, both the techniques correctly characterize the dynamics. Diffusive and flow fitting curves are distinguishable (residual plots), leading to different fitting determination coefficients and resulting in good determinations of the dynamic parameters. In the latter case, STICS does not

reveal a speed contribution, indeed the diffusive fitting curve is equal to the flow one and the relative indetermination of the obtained velocity is very high (about 1200%). This points out that the flow term is redundant and the motion is thus characterized as diffusive. Conversely, iMSD detects a small quadratic contribution, distinguishes the curves and subsequently it correctly discriminate the kind of motion.

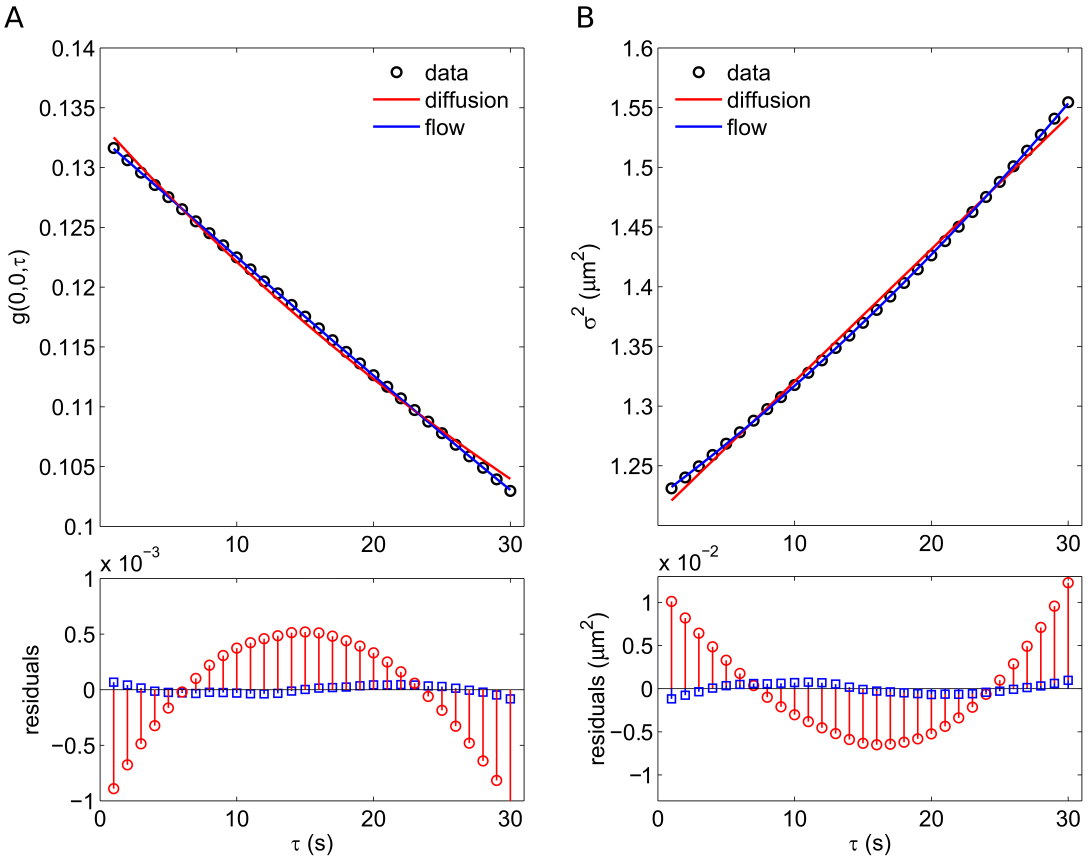

Figure S.5: Fitting profiles and residuals of (A) $g(0,0,\tau)$ and (B) $\sigma^2(\tau)$, adopted by STICS and iMSD techniques, respectively. Analyses were carried out on simulations, under the condition: $\tau_d/\tau_f = 0.12$. Both methods recognize a flow contribution to the investigated dynamics.

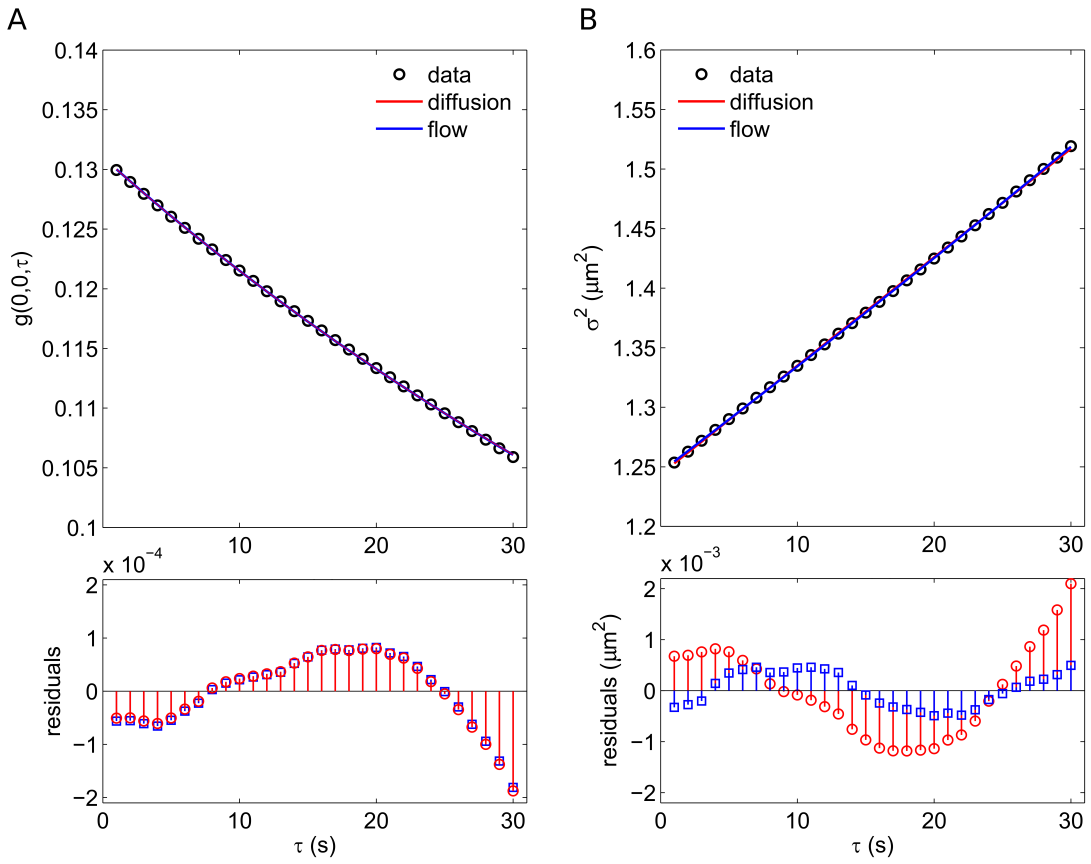

Figure S.6: Fitting profiles and residuals of (A) $g(0,0,\tau)$ and (B) $\sigma^2(\tau)$, adopted by STICS and iMSD techniques, respectively. Analyses were carried out on simulations, under the condition: $\tau_d/\tau_f = 0.06$. STICS does not distinguish a flow contribution to the investigated dynamics (no differences between diffusive and flow fitting curves are detected).

S.3. Slowly changing background

When images are affected by a background, which varies in time with periodicity T_b, the correlation function at zero spatial lag is affected by those oscillation. The amplitude of oscillation depends on the background intensity and may introduce artifacts on the correlation analysis. Indeed, at low Signal to Noise Ratio (SNR), STICS reveals a faster dynamic, due to a shorter decay time of $g(0,0,\tau)$ (Fig. S.7A). Background removal corrects this effect (Fig. S.7B), but it is threshold-dependent and its effectiveness strongly depends on the SNR of the investigated time series (Table S1). On the other side, since no spatial correlation of the background intensity is supposed, temporal oscillations are not detected in the Gaussian variance. Thus iMSD results are more stable, less sensitive to background and their slight underestimation is due to the adopted Gaussian approximation.

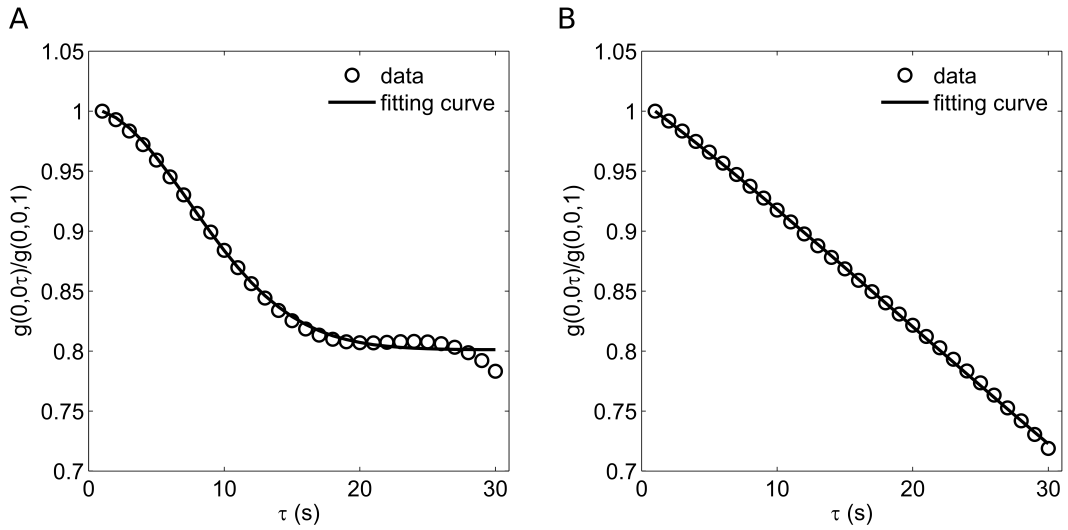

Figure S.7: STICS fitting profiles evaluated on (A) not filtered and (B) filtered movies with a slowly changing background (SNR=6.4). The effect of a slowly changing background is the presence of oscillations in $g(0, 0\tau)$, with strength proportional to the background intensity and same periodicity of the background (in the proposed example $T_b = 30$s).

no filtering

	STICS		iMSD	
SNR	ΔD (%)	Δv (%)	ΔD (%)	Δv (%)
6.40	378	81.8	-10.2	-13.3
12.8	280	41.4	-10.8	-8.95
25.6	106	24.2	-10.3	-8.25
51.2	41.1	18.9	-9.91	-8.05
100	16.1	6.75	-8.93	-7.96

background removal

	STICS		iMSD	
SNR	ΔD (%)	Δv (%)	ΔD (%)	Δv (%)
6.40	86.4	21.3	-7.00	-8.12
12.8	33.5	5.73	-6.08	-6.13
25.6	24.1	4.41	-5.52	-5.83
51.2	11.3	3.76	-5.84	-5.69
100	11.0	3.47	-4.38	-5.64

Table S.1: STICS and iMSD output values of dynamic parameters before and after the background removal. Results are shown as percentage differences from the input data.